Beryllium polyhydride Be$_4$H$_8$(H$_2$)$_2$ synthesized at high pressure and temperature

Takahiro Matsuoka [1,2,*] Hiroshi Fujihisa,[3,†] Takahiro Ishikawa,[4] Takaya Nakagawa,[5] Keiji Kuno,[6] Naohisa Hirao,[7] Yasuo Ohishi,[7] Katsuya Shimizu [8] and Shigeo Sasaki[1]

[1]*Department of Electrical, Electronic and Computer Engineering, Faculty of Engineering, Gifu University, Gifu 501-1193, Japan*
[2]*Material Science and Engineering, Joint Institute for Advanced Materials (JIAM), The University of Tennessee, Knoxville, Tennessee 37996, USA*
[3]*National Institute of Advanced Industrial Science and Technology (AIST), Ibaraki 305-8565, Japan*
[4]*The Elements Strategy Initiative Center for Magnetic Materials, National Institute for Materials Science, Ibaraki 305-0047, Japan*
[5]*Materials Science and Technology Division, Graduate School of Engineering, Gifu University, Gifu 501-1193, Japan*
[6]*Environmental and Renewable Energy Systems Division, Gifu University, Gifu 501-1193, Japan*
[7]*Japan Synchrotron Radiation Research Institute (JASRI), Hyogo 679-5198, Japan*
[8]*Center for Science and Technology under Extreme Conditions, Graduate School of Engineering Science, Osaka University, Osaka 560-8531, Japan*

We report x-ray diffraction and Raman scattering measurements in combination with density functional theory calculations that reveal the formation of beryllium polyhydride Be$_4$H$_8$(H$_2$)$_2$ by the laser heating of a Be-H$_2$ mixture to above 1700 K at pressures between 5 and 8 GPa. Be$_4$H$_8$(H$_2$)$_2$ crystallizes in a $P6_3/mmc$ structure and consists of the corner-sharing BeH$_4$ tetrahedrons and the H$_2$ molecules that occupy an interstitial site. Be$_4$H$_8$(H$_2$)$_2$ is stable at least to 14 GPa upon compression and stable down to 4 GPa at room temperature. Our *ab initio* calculations suggest that Be$_4$H$_8$(H$_2$)$_2$ is a metastable phase of the Be-H system.

I. INTRODUCTION

Since the discovery of beryllium dihydride (BeH$_2$) [1], extensive studies of physical and chemical properties have been performed. Although the toxicity of Be hampers its practical use, the high gravimetric H$_2$ density (H wt% = 18.3%) is attractive for hydrogen storage. Besides, with only six electrons and light mass, BeH$_2$ has been an excellent bench to test advanced quantum molecular calculations [2–6]. Furthermore, significant H wt% makes the investigation of superconductivity appealing because a strong electron-phonon coupling and a high frequency of atomic vibration are anticipated. In these contexts, finding the hydrogen-rich allotropes of the Be-H system is a particular interest. However, there have been no experimental or theoretical studies that have found any stable BeH$_n$ ($n > 2$).

BeH$_2$ has a covalent or a mixed covalent/ionic Be-H bond [7,8]. The ionicity is mainly due to the charge transfer from Be 2s to H 1s atomic orbitals, while the hybridization of H 1s and Be 2p states dominates the covalency [7]. In the solid-state, BeH$_2$ molecules share their H atoms with neighboring BeH$_2$ molecules and form corner-sharing BeH$_4$ tetrahedrons [2,9]. The BeH$_4$ tetrahedrons form two types of BeH$_2$ allotropes at ambient pressure. One is an amorphous BeH$_2$ [10]. Another is a crystalline BeH$_2$ (called α-BeH$_2$) with an *Ibam* (body-centered orthorhombic) struc-

ture. α-BeH$_2$ is synthesized by compacting amorphous BeH$_2$ at high temperatures [11,12]. The phase diagram of BeH$_2$ has been revealed up to 100 GPa at temperatures from 300 to 1500 K by heating the Be-H$_2$ mixture [12]. Pépin and Loubeyre have observed the synthesis of another BeH$_2$ (named β-BeH$_2$, $P4_12_12$ structure) along with α-BeH$_2$ by keeping the Be-H$_2$ mixture at 2.4 GPa and 550 K for several tens of hours [12]. α-BeH$_2$ is stable up to 27 GPa, while β-BeH$_2$ transforms into a different phase (called β'-BeH$_2$) at 17 GPa [12]. Between 27 and 72 GPa, any BeH$_2$ allotrope decomposes into Be and H$_2$ [12]. Be and H$_2$ react again and form a BeH$_2$ that crystallizes in a $P\bar{3}m1$ layered structure (1T structure) at 72 GPa [12]. Any other phases have not been obtained below 1500 K. The Raman scattering measurements on amorphous BeH$_2$ have shown a structural transition at 80 GPa [13]. Theoretical calculations have predicted several structural transformations of BeH$_2$ from the *Ibam* structure, including the transformation to the $P\bar{3}m1$ layered structure, at pressures between 0 and 400 GPa [14–17]. However, a calculation using first-principles variable-composition evolutionary methodology has suggested that BeH$_2$ is the only stable composition up to 400 GPa under static conditions [16]. An evolutionary structure search coupled with density functional theory (DFT) calculation has also predicted that any phases of BeH$_n$ ($n > 2$) are unstable toward decomposition into H$_2$ and BeH$_2$ to at least 250 GPa [17]. According to the calculations, BeH$_2$ remains insulating or semiconducting below 200 GPa [14–16]. Above 200 GPa, *Cmcm* ($P \geqslant 200$ GPa) and $P4/nmm$ ($P \geqslant 350$ GPa) phases exhibit superconducting transitions at temperatures between 20 and 90 K [15,16].

----
*TKMatsuoka08@gmail.com; tmatsuok@utk.edu
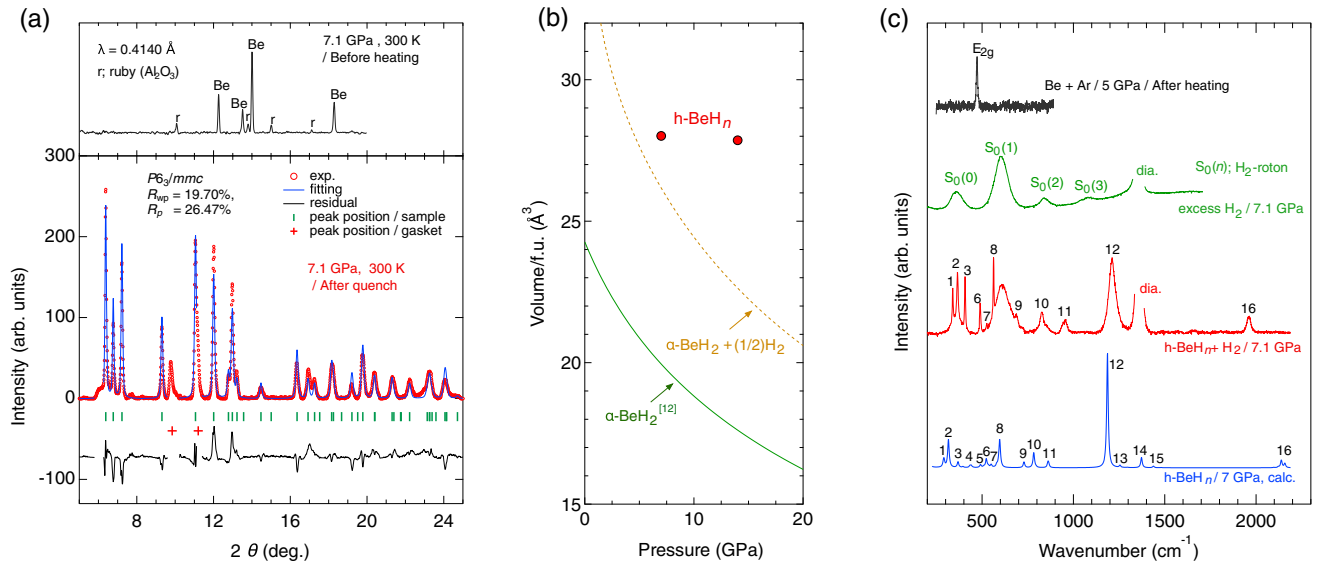†hiroshi.fujihisa@aist.go.jp

FIG. 1. (a) XRD profiles of the Be-H_2 mixture before and after the laser heating with the Rietveld fitting result for the suggested structure model. (b) The $V_{f.u.}$ vs P for h-BeH$_n$ (solid circle), α-BeH$_2$ (solid line), and α-BeH$_2$+(1/2)H$_2$ (dashed line). The $V_{f.u.}$ of α-BeH$_2$ + 1/2(H$_2$) is calculated using the data shown in Refs. [12,24]. The lattice parameters of h-BeH$_n$ at 14 GPa are a = 4.290(1) Å, c = 6.993(2) Å, and V = 111.5(1) Å^3. (c) Raman scattering spectra of the h-BeH$_n$-H$_2$ mixture sample at 7.1 GPa, excess H$_2$, the Be after being heated to 2000 K in Ar at 5 GPa, and the calculated spectrum for Be$_4$H$_8$(H$_2$)$_2$. The numbers indicate the correspondence between the observed and the predicted peaks. "dia." is the signal from a diamond anvil.

This study aims at searching for hydrogen-rich BeH$_n$ ($n > 2$) under high-pressure and high-temperature H$_2$ atmosphere by powder x-ray diffraction (XRD), Raman spectroscopy, and DFT calculation.

II. EXPERIMENTAL DETAILS

In the XRD and Raman scattering measurements, we used a diamond-anvil cell with type-Ia diamond anvils with 0.4 mm culets. We preindented 0.2-mm-thick gaskets made of rhenium (Re) to 50–60 μm and drilled a 150-μm-diameter hole (sample chamber) at the center of the gaskets. We loaded a tiny piece of Be (Sigma-Aldrich, 99.9%) in the sample chamber and filled the remaining room with fluid H$_2$ using a cryogenic H$_2$-loading system [18]. The Be to H$_2$ molar ratios in three independent experiments were between 1:6 and 1:12. We compressed the small chips of ruby (Al$_2$O$_3$:Cr, corundum) together with the sample and estimated the pressure by ruby fluorescence wavelength using a proposed calibration curve [19]. We compressed the Be-H$_2$ mixture at room temperature to pressures between 5 and 8 GPa, and then we heated it to above 1700 K by focusing an IR laser (λ = 1070 nm, SPI laser) on Be. We collected the thermal radiation from the sample and analyzed it in a wavelength between 600 and 800 nm to convert the spectrum to temperature following Planck's blackbody radiation law [20]. The reaction between Be and H$_2$ was detected by monitoring the crystal structure change of Be from hcp using *in situ* XRD measurements at BL10XU/SPring-8. After the hcp structure of Be completely disappeared, we quenched the sample to room temperature. We performed Raman scattering measurements at room temperature in a backscattering geometry by a triple polychromator (JASCO NR1800) equipped with a liquid-

nitrogen-cooled charge-coupled device. The 532-nm radiation from a solid-state laser was used for excitation. The focused laser spot size on the samples was about 10 μm in diameter.

III. RESULTS AND DISCUSSIONS

Figure 1(a) shows the representative XRD profiles before and after the laser heating at 7.1 GPa, together with the result of Rietveld refinement for the suggested structure model discussed later. Note that we first compressed the Be-H$_2$ sample to 7.1 GPa and performed XRD measurements at room temperature [Fig. 1(a), upper panel]. Then, we conducted the laser heating and quenched the sample to room temperature. After quenching, we measured the XRD at room temperature [Fig. 1(a), lower panel]. Before the laser heating, we observed Be and ruby. After the heating, the XRD peaks of Be disappeared, and several new peaks appeared. All of the newly emerged peaks can be indexed with a hexagonal $P6_3/mmc$ structure [a = 4.300(1) Å, c = 6.997(3) Å, and V = 112.05(6) Å], in which Be atoms are at an atomic position (1/3, 2/3, 0.5610) [Z (Be) = 4]. We temporary name this phase h-BeH$_n$. Figure 1(b) is the volume per formula unit ($V_{f.u.}$) vs pressure. The $V_{f.u.}$ is calculated by dividing the unit cell volume by the number of BeH$_2$ units. The $V_{f.u.}$ of h-BeH$_n$ is larger and less compressible than that of α-BeH$_2$ and α-BeH$_2$ + 1/2(H$_2$), suggesting that n exceeds 2.

Figure 1(c) indicates the Raman scattering spectra measured on h-BeH$_n$. Since h-BeH$_n$ was surrounded by excess H$_2$, we observed the signals from both h-BeH$_n$ and solid H$_2$. The Raman scattering peaks from h-BeH$_n$ are easily distinguishable from those of H$_2$ using the data obtained in excess H$_2$. For a control experiment, we heated Be in argon (Ar) to 2000 K at 5 GPa and confirmed that Be kept the hcp structure

TABLE I. Structural parameters for Be$_4$H$_8$(H$_2$)$_2$ at 7.1 GPa. The lattice parameters and the Wyckoff position (Wyck. pos.) of Be were determined from Rietveld refinement. The positions of H atoms were deduced by DFT calculation.

Structure	Atom	Wyck. pos.	x	y	z	Occ.
$P6_3/mmc, Z = 4$	Be	4f	1/3	2/3	0.5610	1
$a = 4.2965(2)$ Å	H	24l	0.3796	0.4135	0.0522	1/4
$c = 7.0095(6)$ Å	H	12j	0.5178	0.2894	1/4	1/6
$V = 112.06$ Å^3	H (mol.[a])	24l	0.0258	0.0076	0.2582	1/12
	H (mol.[a])	24l	0.1790	0.1837	0.3230	1/12

[a]Molecule.

in agreement with previous XRD experiments [21]. In the Raman scattering spectra of h-BeH$_n$, there is a broad peak centering at 1960 cm^{-1}. A theoretical study has calculated that the Be-H stretching mode frequencies of the BeH$_4$ tetrahedron in α-BeH$_2$ are about 1750 (symmetric mode) and 1990 cm^{-1} (antisymmetric mode) [22]. Experimentally, these modes are observed at wave numbers between 1300 and 2000 cm^{-1} for an α and β-BeH$_2$ mixture at 4 GPa, and they shift to higher wave numbers under further compression [12,23]. The observed peak at 1960 cm^{-1} at 7.1 GPa suggests the presence of a BeH$_4$ tetrahedron in the unit cell of h-BeH$_n$.

We performed a structure analysis by indexing, space-group determination, and Rietveld refinement. The diffraction peaks were indexed using BIOVIA Materials Studio (MS) X-CELL software from Dassault Systèmes [27]. The crystal lattice and the atomic coordinates of Be were refined via Rietveld analysis using MS REFLEX software [28]. The energy stability and H-atom positions in each phase were investigated using the DFT program MS CASTEP [29]. We employed the generalized gradient approximation–Perdew-Burke-Ernzerhof for solids (PBEsol) exchange-correlation functionals [30] and used ultrasoft pseudopotentials [31]. The lattice parameters were set to the experimental values and refined by Rietveld analysis, and the atomic positions were optimized to minimize the total energy. When we restricted the stoichiometry to BeH$_2$, we obtained two models: $P31c$ and $P\bar{6}c2$ structures that were composed of corner-sharing four BeH$_4$ tetrahedrons. However, the stress estimated by our DFT for these two models became 0 GPa in disagreement with experimental results (7.1 GPa). We note that these two models are isotypical to ice-Ih (ice at atmospheric pressure). Besides, the $V_{f.u.}$ of h-BeH$_n$ is bigger than that of α-BeH$_2$ by more than 7 Å^3 at 7.1 GPa [Fig. 1(b)]. Also, h-BeH$_n$ is less compressible than α-BeH$_2$. To mechanically support such a crystal structure with large internal space at pressures as high as 14 GPa, the presence of some substance in the interstitial sites is strongly suggested. Considering that H$_2$ surrounds h-BeH$_n$ in the sample chamber, a H atom or an H$_2$ molecule is the most probable. When H atoms were at the interstitial sites of the $P31c$ and $P\bar{6}c2$ structures, our DFT calculation and MD simulation calculated that BeH$_4$ tetrahedrons decomposed, and the unit cells collapsed. When H$_2$ molecules were at the interstitial sites, an excellent fit to the experimental XRD profile was obtained, and the crystal structure became stable in the DFT calculation. The best structure model to describe h-BeH$_n$ including the disorders of H and H$_2$ is summarized in Table I. Note that the lattice parameters and the atomic position of Be were determined from Rietveld refinement. The

positions of H atoms were deduced by DFT calculation. In Fig. 2, we show the visualized structure model. The BeH$_4$ tetrahedrons rotationally oscillate, and the unit cell goes back and forth between $P31c$ and $P\bar{6}c2$. The H$_2$ molecules freely rotate. See Movie 1 in the Supplemental Material for the rotational oscillations of BeH$_4$ units and H$_2$ molecules [26].

We thought of the possible occupation of the interstitial sites by Al and O from ruby, Re from the gasket, and carbon (C) from diamond anvils during the laser heating. However, if such heavier atoms are included, the XRD measurements and the following analysis allow us to detect them. Therefore, we exclude the occupation by C, O, and Al.

To examine the crystal structure model of h-BeH$_n$, we compare the calculated Raman spectra for the suggested structure model with experimental results at 7.1 GPa [Fig. 1(c)]. We note that we employed a fully ordered structure with space group $P1$ to do the calculation. Peak 16 consists of eight peaks originating from Be-H stretching modes (see Supplemental Movie 2 [26] for the Be-H stretching mode at 2138 cm^{-1}), and two of them at 2138 and 2157 cm^{-1} are more intense than others. We assume that the eight peaks overlap and form the observed single broad peak. Peak 12 (1186 cm^{-1}) is the rotational mode of the BeH$_4$ tetrahedron (see Supplemental
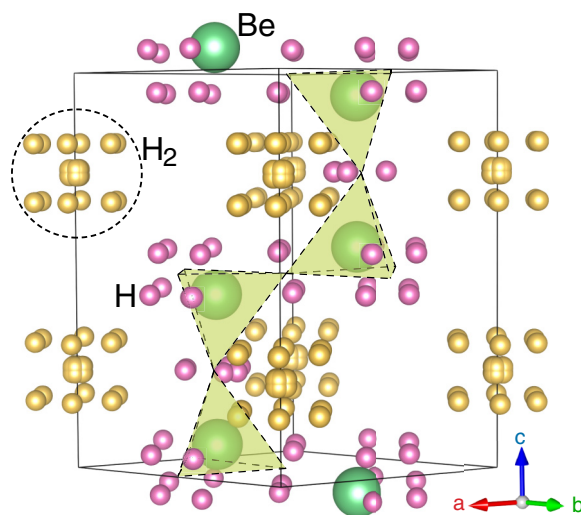

FIG. 2. Be$_4$H$_8$(H$_2$)$_2$ (visualized using VESTA [25]). Hydrogen atoms "H" are moving around the disordered positions. The H$_2$ atoms are rotating in a dotted circle. Each tetrahedron is a corner-sharing BeH$_4$ unit. See the Supplemental material for the crystal structure information file (CIF) of Be$_4$H$_8$(H$_2$)$_2$ [26].
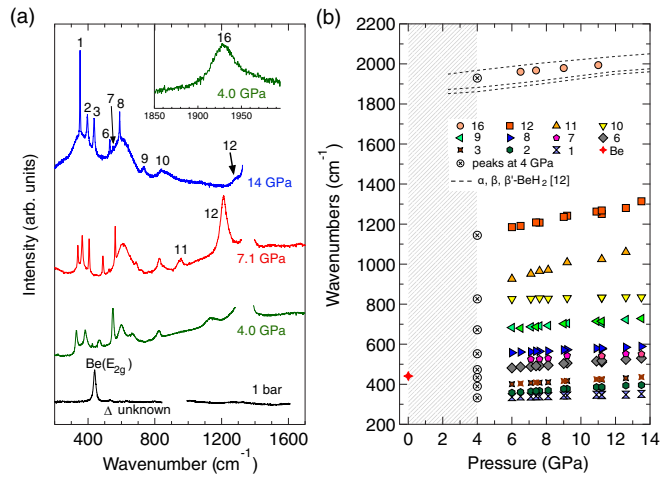
FIG. 3. (a) The Raman scattering spectra of h-BeH$_n$ as pressure decreases. The numbers indicate the peaks described in Fig. 1(c). The spectra at 1 bar were measured after the diamond anvil was removed. (b) The pressure dependence of the Raman shifts for peaks 1–16. The data obtained in three independent experiments are plotted together. Below 4 GPa (shaded area), h-BeH$_n$ is unstable at room temperature.

Movie 3 [26] for the rotation that corresponds to 12). The appearance of peaks 12 and 16 in the experiments strongly supports the suggested structure model. In the hydrides that consist of H$_2$, we sometimes observe the intra-H$_2$ stretching mode (vibron) at wave numbers shifted from that of pure H$_2$ (4200–4400 cm^{-1}). In the present experiments, we did not observe the additional peaks near the vibron of excess H$_2$. We speculate that the peak from the accommodated H$_2$ in h-BeH$_n$ overlaps with that of the excess H$_2$. Although a perfect matching is not achieved, the relative intensities and relative positions of the observed and calculated peaks are in reasonable agreement as a whole. We conclude that h-BeH$_n$ is Be$_4$H$_8$(H$_2$)$_2$ with the $P6_3/mmc$ structure that is composed of BeH$_4$ tetrahedrons and H$_2$.

We investigated the structural stability of h-BeH$_n$ upon pressure decrease to 1 bar by monitoring the structure change using Raman scattering measurement [Figs. 3(a) and 3(b)]. We obtained the reproducible results from three independent experiments. As pressure decreases, Raman scattering peaks show a monotonic decrease to 6.0 GPa [Fig. 3(b)]. When the pressure reaches 4.0 GPa, peaks 3 and 11 disappear, a peak appears at 432 cm^{-1}, and other peaks become broad. However, the sample still maintains peaks 16 and 12, suggesting that the BeH$_4$ tetrahedron persists at 4.0 GPa. At 1 bar, the peaks from h-BeH$_n$ vanish, and the peaks from Be metal and an unknown peak remain. Judging from the peak position, we consider that the possible origin of the unknown phase is the luminescence of ruby, covering the 100–800 cm^{-1} region, that was there nearby the sample [32]. We conclude that h-BeH$_n$ is unstable below 4 GPa decomposing to Be and H$_2$.

Regarding the synthesis condition and the stability region of h-BeH$_n$, we note the following. In the present experiment, our laser heating was limited between 5 and 8 GPa. The synthesis condition remains to be cleared. The stability region

has a lower limit of 4 GPa. On the other hand, the upper limit is not known.

Here, we compare the crystal structure of h-BH$_n$ with that of α-BeH$_2$ and discuss the Be-H bonding. Both h-BeH$_n$ and α-BeH$_2$ consist of BeH$_4$ tetrahedrons. The difference is in the positions of shared H atoms. In α-BeH$_2$ at 1 bar, the H-Be-H connection is bent about 130°, and a Be-H distance is 1.38 Å, while another is 1.41 Å [12]. In h-BeH$_n$, the Be-H-Be angle is near 180°. The H atoms are at the midpoint between two Be atoms, and the Be-H distance (1.44 Å at 7 GPa) is longer than that of α-BeH$_2$. Another difference is in the structural stability at 1 bar. Contrary to the stability of α-BeH$_2$, h-BeH$_n$ decomposes. We think that the shared H atom is not tightly bonded to a single Be atom, and the Be-H bond in h-BeH$_n$ is possibly not a covalent. We speculate that the accommodated H$_2$ molecules mechanically support the unit cell of h-BeH$_n$ and also elongate the Be-H bond to the extent the bond loses covalency.

To go into the interaction between H$_2$ and the surrounding BeH$_4$ tetrahedrons, we also compare the crystal structure of h-BeH$_n$ with the compound of water ice and helium (He hydrate). Teeratchanan and Hermann have performed the first principle study assuming van der Walls interaction between He and H$_2$O with a binding energy of -7.99 meV and predicted the formation of He hydrate with ice-Ih structure where He occupies the interstitial site (cage) [33]. From the similarity of the crystal structure and the free rotation of H$_2$, we speculate that the interaction between H$_2$ and BeH$_2$ is similar to that of the He hydrate.

To obtain further knowledge about the thermodynamical stability of Be$_4$H$_8$(H$_2$)$_2$, we searched for the most stable crystal structure under static conditions using a genetic algorithm and first-principles calculations (see the Supplemental Material [26]). Our structure search predicts that BeH$_3$ has a positive formation enthalpy of 12 mRy/atom at 20 GPa for decomposition into BeH$_2$ and H$_2$, as is the case in the theoretical results reported earlier [14–17]. Besides, a triclinic $P\bar{1}$ structure emerges as the most stable one instead of $P6_3/mmc$ observed by experiments. From our theoretical calculation, it is implicated that Be$_4$H$_8$(H$_2$)$_2$ with $P6_3/mmc$ is a metastable phase that is stabilized dynamically by the thermal effect at finite temperature.

The notable characteristic of h-BeH$_n$ is the anomalous incompressibility of $V_{f.u.}$ compared to that of α-BeH$_2$ and α-BeH$_2 + 1/2(H_2)$ [Fig. 1(b)]. The difference in $V_{f.u.}$ between h-BeH$_n$ and α-BeH$_2 + 1/2(H_2)$ becomes larger as the pressure increases. As discussed, h-BeH$_n$ is a dynamically stabilized phase whose formation enthalpy is unfavorable, compared to α-BeH$_2$ and α-BeH$_2 + 1/2(H_2)$. To keep such metastable h-BeH$_n$ under increasing pressure, it is required to decrease the internal energy. At a given pressure and temperature, materials behave to minimize the Gibbs free energy $G = U + PV - TS$. The PV term is dominant under high pressure, and the V of h-BeH$_n$ is required to be comparable to or less than that of the α-BeH$_2$-H$_2$ mixture. For hydrides, variable occupancy is common [34,35]. For example, hydrogen clathrate, in which hydrogen molecules are trapped within cages formed from water molecules, in a manner not dissimilar to the structure of h-BeH$_n$, has a cage occupancy that varies by a factor of 1.5 [35]. Therefore, it would be appropriate to assume that

the n in h-BeH$_n$ possibly increases with pressure so that the $V_{f.u.}$ of h-BeH$_n$ approaches that of α-BeH$_2$ + $x/2$(H$_2$), where $x/2$ is the number of the inserted H$_2$ per formula unit. We expect future neutron scattering experiments will give us a clear answer.

IV. SUMMARY

In summary, $Be_4H_8(H_2)_2$ is formed by applying high pressure (5–8 GPa) and high temperature (above 1700 K) to the Be-H$_2$ mixture. In $Be_4H_8(H_2)_2$, BeH$_4$ tetrahedrons form a hexagonal $P6_3/mmc$ structure, and there are H$_2$ molecules in the interstitial sites. The observed $Be_4H_8(H_2)_2$ is possibly a metastable phase in the Be-H phase diagram. The H atoms are not covalently bonded to Be atoms. The present results would motivate further studies such as searching for superconductivity and recovering $Be_4H_8(H_2)_2$ to ambient pressure. So far, there has been no prediction of the formation of $Be_4H_8(H_2)_2$.

Revealing the phase diagram of the Be-H system would be a particular interest, extending pressure and temperature ranges. The behavior of h-BeH$_n$ between 27 and 70 GPa should be investigated, because Be + H$_2$ is reported to be more stable than α-BeH$_2$ [12]. Those studies would contribute to understanding the Be-H interaction, which has not been fully understood for years.

[1] G. D. Barbaras, C. Dillard, A. E. Finholt, T. Wartik, K. E. Wilzbach, and H. I. Schlesinger, J. Am. Chem. Soc. **73**, 4585 (1951).

[2] S. Sampath, K. M. Lantzky, C. J. Benmore, J. Neuefeind, J. E. Siewenie, P. A. Egelstaff, and J. L. Yarger, J. Chem. Phys. **119**, 12499 (2003).

[3] E. N. Koukaras, A. P. Sgouros, and M. M. Sigalas, J. Am. Chem. Soc. **138**, 3218 (2016).

[4] T. Hrenar, H.-J. Werner, and G. Rauhut, Phys. Chem. Chem. Phys. **7**, 3123 (2005).

[5] C. Bheema Lingam, K. Ramesh Babu, S. P. Tewari, and G. Vaitheeswaran, Comput. Theor. Chem. **963**, 371 (2011).

[6] L. N. Vidal and P. A. M. Vazquez, Chem. Phys. **321**, 209 (2006).

[7] N. N. Greenwood and A. Earnshaw, in *Chemistry of the Elements*, 2nd ed. (Pergamon Press, Oxford, 1997), p. 115.

[8] B.-T. Wang, P. Zhang, H.-L. Shi, B. Sun, and W.-D. Li, Eur. Phys. J. B **74**, 303 (2010).

[9] S. V. Marchenko, V. F. Petrunin, Y. E. Markushkin, M. D. Senin, and N. A. Chirin, Sov. Phys. Solid State **24**, 1308 (1982).

[10] G. J. Brendel, E. M. Marlett, and L. M. Niebylski, Inorg. Chem. **17**, 3589 (1978).

[11] G. S. Smith, Q. C. Johnson, D. K. Smith, D. Cox, R. L. Snyder, R.-S. Zhou, and A. Zalkin, Solid State Commun. **67**, 491 (1988).

[12] C. M. Pépin and P. Loubeyre, Phys. Rev. B **93**, 224104 (2016).

[13] S. Nakano, M. Ahart, J. L. Yarger, H.-k. Mao, and R. J. Hemley, Special Issue Rev. High Press. Sci. Technol. **15**, 261 (2005).

[14] P. Vajeeston, P. Ravindran, A. Kjekshus, and H. Fjellvåg, Appl. Phys. Lett. **84**, 34 (2004).

[15] Z. Wang, Y. Yao, L. Zhu, H. Liu, T. Iitaka, H. Wang, and Y. Ma, J. Chem. Phys. **140**, 124707 (2014).

[16] S. Yu, Q. Zeng, A. R. Oganov, C. Hu, G. Frapper, and L. Zhang, AIP Adv. **4**, 107118 (2014).

[17] J. Hooper, B. Altintas, A. Shamp, and E. Zurek, J. Phys. Chem. C **117**, 2982 (2013).

[18] Z. Chi, H. Nguyen, T. Matsuoka, T. Kagayama, N. Hirao, Y. Ohishi, and K. Shimizu, Rev. Sci. Instrum. **82**, 105109 (2011).

[19] H. K. Mao, J. Xu, and P. M. Bell, J. Geophys. Res. **91**, 4673 (1986).

[20] Y. Ohishi, N. Hirao, N. Sata, K. Hirose, and M. Takata, High Press. Res. **28**, 163 (2008).

[21] A. Lazicki, A. Dewaele, P. Loubeyre, and M. Mezouar, Phys. Rev. B **86**, 174118 (2012).

[22] U. Hantsch, B. Winkler, and V. Milman, Chem. Phys. Lett. **378**, 343 (2003).

[23] S. Sampath, A. I. Kolesnikov, K. M. Lantzky, and J. L. Yarger, J. Chem. Phys. **128**, 134512 (2008).

[24] P. Loubeyre, R. LeToullec, D. Hausermann, M. Hanfland, R. J. Hemley, H. K. Mao, and L. W. Finger, Nature (London) **383**, 702 (1996).

[25] K. Momma and F. Izumi, J. Appl. Cryst. **44**, 1272 (2011).

[26] See Supplemental Material at http://link.aps.org/supplemental/10.1103/PhysRevMaterials.4.125402 for Movies 1–3 and the CIF for $Be_4H_8(H_2)_2$.

[27] M. A. Neumann, J. Appl. Cryst. **36**, 356 (2003).

[28] Dassault Systèmes Americas Corp., BIOVIA Materials Studio Reflex website, https://www.3ds.com/products-services/biovia/products/molecular-modeling-simulation/biovia-materials-studio/analytical-and-crystallization/, accessed: 2020-09-24.

[29] S. J. Clark, M. D. Segall, C. J. Pickard, P. J. Hasnip, M. I. J. Probert, K. Refson, and F. C. Payne, Z. Kristallogr. **220**, 567 (2005).

[30] J. P. Perdew, A. Ruzsinszky, G. I. Csonka, O. A. Vydrov, G. E. Scuseria, L. A. Constantin, X. Zhou, and K. Burke, Phys. Rev. Lett. **100**, 136406 (2008).

[31] D. Vanderbilt, Phys. Rev. B **41**, 7892 (1990).

[32] K. Syassen, High Press. Res. **28**, 75 (2008).

[33] P. Teeratchanan and A. Hermann, J. Chem. Phys. **143**, 154507 (2015).

[34] T. Matsuoka, H. Fujihisa, N. Hirao, Y. Ohishi, T. Mitsui, R. Masuda, M. Seto, Y. Yoda, K. Shimizu, A. Machida, and K. Aoki, Phys. Rev. Lett. **107**, 025501 (2011).

[35] K. A. Lokshin, Y. Zhao, D. He, W. L. Mao, H.-K. Mao, R. J. Hemley, M. V. Lobanov, and M. Greenblatt, Phys. Rev. Lett. **93**, 125503 (2004).